Fermi National Accelerator Laboratory

FERMILAB-Pub-94/038-E

E772

Cross Sections for the Production of High-Mass Muon Pairs from 800 GeV Proton Bombardment of ^2H

P.L. McGaughey et al
The E772 Collaboration

Fermi National Accelerator Laboratory
P.O. Box 500, Batavia, Illinois 60510

February 1994

Submitted to *Physical Review D*

Operated by Universities Research Association Inc. under Contract No. DE-AC02-76CHO3000 with the United States Department of Energy

Disclaimer

Cross Sections for the Production of High-Mass Muon Pairs from 800 GeV Proton Bombardment of ^2H

P. L. McGaughey, J. M. Moss, D. M. Alde, H. W. Baer, T. A.Carey, G. T. Garvey, A. Klein,C. Lee, M. J. Leitch, J. Lillberg, C. S. Mishra, J. C. Peng,
Los Alamos National Laboratory, Los Alamos, New Mexico 87545

C. N. Brown, W. E. Cooper, Y. B. Hsiung,
Fermilab, Batavia, Illinois 60510

M. R. Adams,
University of Illinois at Chicago, Chicago, Illinois 60680

R. Guo, D. M. Kaplan,
Northern Illinois University, DeKalb, Illinois 60115

R. L. McCarthy,
SUNY at Stony Brook, Stony Brook, New York 11794-3800

G. Danner, M. Wang,
Case Western Reserve University, Cleveland, Ohio 44106

and

M. Barlett, G. Hoffmann,
University of Texas, Austin, Texas 78712

Abstract

Absolute cross sections as functions of kinematic variables are presented for the production of muon pairs from 800 GeV proton bombardment of ^2H. Drell-Yan (continuum) dimuons were recorded in the mass regions $4.5 \leq M_{\mu^+\mu^-} \leq 9\ GeV$ and $M_{\mu^+\mu^-} \geq 11\ GeV$, with an x-Feynman range $-0.1 \leq x_F \leq 0.75$. This range corresponds to smaller masses and larger values of x_F than previous 800 GeV Drell-Yan data. Cross sections for the Υ (1S) resonance are also given versus transverse momentum and x_F.

PAC numbers: 13.85Qk, 12.38Qk, 25.40Ve

I. Introduction

Continuum lepton pair production in high-energy hadron collisions, known as the Drell-Yan (DY) process[1], has been studied experimentally for many years, and with the advent of quantum chromodynamical (QCD) descriptions including next-to-leading-order corrections, can be characterized as very well understood theoretically[2]. Phenomenological evaluations of parton structure functions now often use DY data as well as data from deep-inelastic lepton scattering (DIS).

Experimentally in addition to continuum pair production, one observes lepton pair decay of the J/ψ and Υ families of quarkonia. The mechanism of hadronic production of these states has been extensively studied using QCD phenomenology. The dominant mechanism appears to be gluon fusion processes at 800 GeV[3].

In this paper we present a detailed analysis of cross section data for dimuon production from 800 GeV proton bombardment of ^2H from Fermilab E772. Previous E772 publications have dealt with the atomic mass dependence of DY[4, 5], J/ψ and ψ' [6], and Υ [7] production. Because of uncertainties in magnetic field maps which affect only the low mass region of the spectrometer acceptance, we do not give cross sections for the J/ψ and ψ' resonances.

II. Experimental Apparatus

Experiment 772 used a modified version of the large spectrometer in the Meson-East beamline at Fermilab which was originally constructed for Experiment 605[8]. A complete description of the E605 apparatus and its operation in the dimuon configuration has been published recently[8], hence we will detail only the essential differences which apply to E772. The spectrometer consisted of a target chamber followed by three dipole magnets and detection elements described briefly below. The primary proton beam passed through the target and was attenuated in a beam dump located inside the second large dipole. The magnetic fields of the three dipole magnets of the spectrometer were configured to optimize acceptance for three different regions of dimuon mass with low-mass thresholds roughly at 3, 4.5, and 6 GeV. The spectrometer was used in a closed-aperture configuration; a thick hadron absorber in front of the first active detector permitted incident proton intensities of 10^{11} protons per second at the high-mass magnet setting and 3×10^{10} at the low-mass setting. The tracking system consisted of three stations of multiwire proportional chambers and drift chambers. Triggering was achieved using hodoscope stations configured in quadrants covering the spectrometer acceptance. Muon identification was accomplished with further stations of hodoscopes and proportional tubes located beyond a thick absorber wall.

III. Targeting and Data Collection

The 800 GeV proton beam, 8 mm wide by ≤ 2 mm high at the target, was monitored by position sensitive RF cavities and ion chambers; position stability was typically better than 1 mm. Beam intensity was monitored by two secondary-emission detectors and a quarter-wave RF cavity. Two four-element scintillator telescopes viewing the target at 90° monitored the luminosity, the beam duty factor, and the data acquisition livetime. Although E772 recorded data on five different targets, only the ^2H data are included in the present paper. As will be apparent below, the statistical precision of the ^2H data is sufficient in comparison with the dominant systematic errors. The ^2H target was a 50.7 cm long by 7.6 cm diameter cryogenic cell. The beam entered and exited through 51 μm stainless steel windows. The target was operated at a temperature of 24 K with a typical density of 8.24 g/cm^2. The target density was monitored by an accurate measurement of the vapor pressure in the cell above the liquid.

The first level trigger was formed by requiring a coincidence of hodoscope signals on the left and right halves of the spectrometer, including the final plane located behind the second absorber wall. A second trigger level employed fast lookup tables to require a pair of hodoscope roads which were consistent with two muons originating at the target and traversing the spectrometer aperture. This level was essential in achieving significant discrimination against the dominant rate of muons from the beam dump. A third trigger level, employing a fast trigger processor evaluation of wire chamber tracking[8], was employed to tag data on tape for fast computer analysis, but not to reject events.

The event rate to tape was typically $\approx$ 100 per 20-second-long beam spill, with roughly 2% being good target events. Overall livetimes were usually in excess of 98%. A total of 83080 muon pairs were recorded from ^2H in the DY region, defined as $4.5 \leq M_{\mu^+\mu^-} \leq 9\ GeV$ or $M_{\mu^+\mu^-} \geq 11\ GeV$. These requirements safely excluded J/ψ and Υ contributions. A total of 4410 Υ events were recorded from the ^2H target. Details of the procedure used to fit the peaks in the Υ region have been given in a previous publication[7].

IV. Data Analysis and Normalization

Track reconstruction was performed with the aid of a Fermilab Advanced

Computing Project parallel processor. Energy loss and multiple scattering corrections were used to improve the mass resolution. Track pair reconstruction efficiency averaged ≈94%. Other sources of inefficiency include the live time (≈99%) and trigger efficiency (≈94%). A small contamination (≈3%) of random muon coincidences was subtracted by studying like-sign muon pairs. Target-out backgrounds were measured to be below the 1% level. Beam spills were carefully monitored; those with poor livetime, duty factor, beam position, etc., were discarded.

Differential cross sections are calculated for kinematic variable Ω using

$$\frac{d\sigma}{d\Omega}\bigg|_{\Omega=\langle\Omega\rangle} \equiv \frac{1}{\mathcal{L}}\frac{N_{ev}}{a\epsilon}\frac{1}{\Delta\Omega} \tag{1}$$

where N_{ev} is the number of events in $\Delta\Omega$, a is the acceptance, ϵ is the detection efficiency and $\mathcal{L}$ is the integrated luminosity. The detection efficiency is the product of the livetime and track reconstruction and trigger efficiencies, which were given above. The effective luminosity per target nucleon was calculated as

$$\mathcal{L} = \mathrm{N_0}\rho\lambda(1 - \mathrm{e}^{-\mathrm{L}/\lambda})\mathrm{N_{inc}} \tag{2}$$

where N_0 is Avogadro's number, ρ, L and λ are the density, length and hadronic absorption length of the ^2H target, respectively, and $\mathrm{N_{inc}}$ is the number of beam protons intercepted by the target. The integrated luminosity for the ^2H measurements reported here was $(5.8 \pm 0.3) \times 10^{40}$ nucleon / cm^2.

The acceptance was calculated using a Monte Carlo simulation of the spectrometer. Roughly 10^6 muon pairs were tracked through the simulated spectrometer. Events were required to satisfy the trigger condition. These events were digitized, then reconstructed using an analysis identical to that used with the actual experimental data. Event generators were tuned to give an accurate representation of Drell-Yan and resonance decays. The acceptance is defined as the ratio of reconstructed events to generated events.

The systematic error in the cross sections reported below is dominated by the uncertainty in the acceptance (8%), luminosity (5%), trigger efficiency (3%) and reconstruction efficiency (1%). The estimated overall systematic error is $\approx \pm 10\%$. The uncertainty in the acceptance is mainly due to limitations in the knowledge of the magnetic field in the region between the first two magnets.

V. Drell-Yan Cross Sections

The parton-model cross section for the DY process is given by,

$$M^3 \frac{d^2\sigma}{dM dx_F} = \frac{8\pi\alpha^2}{9} \frac{x_1 x_2}{x_1 + x_2} \times \sum_i e_i^2 [q_i(x_1)\bar{q}_i(x_2) + \bar{q}_i(x_1) q_i(x_2)], \tag{3}$$

where α is the fine-structure constant, e_i the electric charge of a quark or antiquark of flavor i, and $q_i(\bar{q}_i)$ are quark (antiquark) structure functions. The kinematics of parton-parton fusion also lead to the relations,

$$\tau \equiv M^2/s = x_1 x_2,$$

$$x_F \equiv x_1 - x_2 = 2p_l/\sqrt{s}. \tag{4}$$

Here, $\sqrt{s}$ is the NN center-of-mass energy and p_l is the longitudinal momentum of the of the virtual photon of mass M.

The above relations are easily extended to account for the evolution of quark structure functions with Q^2. In recent years next-to-leading order QCD calculations[2] have been very successful in accounting for the large correction factor (the so-called "K" factor, with $K \approx 2$) previously required to bring the parton formula into agreement with experiment. The higher order QCD contributions also account for the experimentally observed p_T distributions, which extend to much larger values than can be accounted for by the transverse momenta of quarks in the nucleon.

Tests have also been made of the angular distribution of dileptons from DY production, expected in lowest order to behave as $1 + cos^2\theta$. Our experimental acceptance was sufficiently limited in $\theta_{\mu\mu}$ to yield no further useful tests of this relationship.

Figures 1 and 2 compare the cross sections of E772 and E605[8] in terms of $M^3 \frac{d^2\sigma}{dMdx_F}$ per nucleon versus M and x_F. Only statistical errors are shown in the figures. It is clear that the present data cover a larger range of x_F and smaller values of dimuon mass. Figures 3 and 4 show a larger sample of the E772 data which is listed completely in table I.

Table II and Fig. 5 display the p_t dependence of the DY data in terms of the invariant cross section,

$$E\frac{d^3\sigma}{dp^3} = \frac{2E}{\pi\sqrt{s}}\frac{d^2\sigma}{dp_t^2 dx_F}. \tag{5}$$

An earlier publication[4] showed cross sections integrated over x_F with a misleading figure label. Figure 1 of Ref.[4] should have indicated the x_F range -0.2 to 0.8 instead of the the entire x_F range. Even with this correction the cross section data of Ref.[4] should not be used. The data analysis presented here includes a more precise understanding of the trigger efficiency than was available previously. In addition we now believe that uncertainties in the magnetic field maps may lead to additional errors near the edges of the acceptance; these uncertain regions have been excluded here.

VI. Upsilon(1S) Cross Sections

Because of the extended target used in E772 the mass resolution was poorer that achieved in E605[8]. Nevertheless it was sufficient[7] to completely resolve the Υ from the Υ' and Υ'' states. Thus we report cross sections times the branching ratio into dimuons for the $\Upsilon(1S)$ only. These are given in tables III and IV versus x_F and p_t respectively. The cross sections reported here are not directly comparable to those of E605[8] due to the large measured nuclear dependence[7] of the Υ resonance.

References

[1] S.D. Drell and T-M. Yan., Phys. Rev. Lett.**25**, 316(1970).

[2] W.J. Stirling and M.R. Whalley, Journal of Phys. **G 19**, D1(1993).

[3] W-Y.P. Hwang, J.M. Moss, and J.C. Peng, Phys. Rev. **D 38**, 2785(1988), and references therein.

[4] D. M. Alde et al., Phys. Rev. Lett. **64**, 2479(1990).

[5] P. L. McGaughey et al., Phys. Rev. Lett. **69**, 1726(1992).

[6] D. M. Alde et al., Phys. Rev. Lett. **66**, 133(1991).

[7] D. M. Alde et al., Phys. Rev. Lett. **66**, 2285(1991).

[8] G. Moreno et al., Phys. Rev. **D 43**, 2815(1991), and references therein.

Figure Captions

Figure 1. Comparison of E772 (solid squares) with E605[8] (open squares) Drell-Yan cross sections per nucleon versus dimuon mass for the bin $x_F = 0.125$. Only statistical errors are shown. The data correspond to the format of Table I (x_F bins 0.05 wide and mass bins 0.5 GeV wide). The points are plotted at the center of each bin.

Figure 2. Comparison of E772 (solid squares) with E605[8] (open squares) Drell-Yan cross sections per nucleon versus x_F for the mass bin 8.25 GeV. Only statistical errors are shown. The data correspond to the format of the Table I (x_F bins 0.05 wide and mass bins 0.5 GeV wide). The points are plotted at the center of each bin.

Figure 3. E772 Drell-Yan cross sections per nucleon, $m^3 d^2\sigma/dm dx_F$ ($nb \times GeV^2$) for bins with $x_F = 0.125$, 0.225, 0.325, and 0.425 (top to bottom). The lower three data sets have been divided by factors of 10, 100, and 1000, respectively. Only statistical errors are shown. The data correspond to the format of the Table I (x_F bins 0.05 wide and mass bins 0.5 GeV wide). The points are plotted at the center of each bin.

Figure 4. Drell-Yan cross sections per nucleon, $m^3 d^2\sigma/dm dx_F$ ($nb \times GeV^2$) for bins with $M = 5.75$, 8.25, and 11.25 GeV. (top to bottom). Only statistical errors are shown. The data correspond to the format of the Table I (x_F bins 0.05 wide and mass bins 0.5 GeV wide). The points are plotted at the center of each bin.

Figure 5. Drell-Yan cross sections per nucleon, $E \times d^3\sigma/dp^3(pb/GeV^2)$, for 1 GeV-wide mass bins centered at M = 5.5 GeV (solid circles), 8.5 GeV (open circles), and 11.5 GeV (diamonds). Cross sections are for the interval $0.1 \leq x_F \leq 0.3$.

Table I. Scaling form of the Drell-Yan cross section, $m^3 d^2\sigma/dmdx_F$ in $nb \times GeV^2$/nucleon. Only statistical errors are listed; total error includes an additional $\pm 10\%$ systematic error described in the text.

Mass(GeV)	$x_F = 0.025$	Error	$x_F = 0.075$	Error
4.75	.210E+02	.170E+01	.227E+02	.117E+01
5.25	.187E+02	.139E+01	.180E+02	.954E+00
5.75	.165E+02	.130E+01	.138E+02	.664E+00
6.25	.931E+01	.640E+00	.109E+02	.514E+00
6.75	.751E+01	.549E+00	.872E+01	.451E+00
7.25	.571E+01	.474E+00	.819E+01	.472E+00
7.75	.683E+01	.585E+00	.494E+01	.313E+00
8.25	.355E+01	.350E+00	.412E+01	.295E+00
8.75	.340E+01	.330E+00	.363E+01	.281E+00
11.25	.167E+01	.419E+00	.126E+01	.301E+00
11.75	.928E+00	.325E+00	.707E+00	.194E+00
12.25	.600E+00	.266E+00	.286E+00	.126E+00
12.75	.308E+00	.231E+00	.897E+00	.387E+00
13.25	.463E+00	.293E+00	.543E+00	.273E+00
13.75	.152E+00	.160E+00	.145E+00	.151E+00
14.25	.290E+01	.359E+01	.139E+00	.146E+00
Mass(GeV)	$x_F = 0.125$	Error	$x_F = 0.175$	Error
4.75	.212E+02	.970E+00	.214E+02	.987E+00
5.25	.177E+02	.686E+00	.159E+02	.508E+00
5.75	.128E+02	.474E+00	.120E+02	.383E+00
6.25	.107E+02	.407E+00	.101E+02	.348E+00
6.75	.849E+01	.369E+00	.788E+01	.301E+00
7.25	.732E+01	.342E+00	.712E+01	.305E+00
7.75	.600E+01	.322E+00	.501E+01	.247E+00
8.25	.477E+01	.287E+00	.433E+01	.238E+00
8.75	.400E+01	.276E+00	.400E+01	.253E+00
11.25	.146E+01	.240E+00	.748E+00	.168E+00
11.75	.840E+00	.216E+00	.385E+00	.101E+00
12.25	.548E+00	.181E+00	.456E+00	.121E+00
12.75	.406E+00	.153E+00	.619E+00	.190E+00
13.25	.381E+00	.189E+00	.996E-01	.609E-01
13.75	.225E+00	.174E+00	.771E-01	.468E-01
14.25	.394E+00	.306E+00	.155E+00	.118E+00
14.75	.863E-01	.899E-01	.388E+00	.200E+00

Mass(GeV)	$x_F = 0.225$	Error	$x_F = 0.275$	Error
4.75	.188E+02	.105E+01	.174E+02	.122E+01
5.25	.142E+02	.427E+00	.126E+02	.397E+00
5.75	.112E+02	.349E+00	.105E+02	.347E+00
6.25	.853E+01	.290E+00	.748E+01	.268E+00
6.75	.673E+01	.258E+00	.578E+01	.224E+00
7.25	.674E+01	.284E+00	.509E+01	.222E+00
7.75	.502E+01	.234E+00	.423E+01	.213E+00
8.25	.416E+01	.221E+00	.376E+01	.205E+00
8.75	.373E+01	.226E+00	.316E+01	.199E+00
11.25	.116E+01	.190E+00	.103E+01	.151E+00
11.75	.774E+00	.158E+00	.745E+00	.140E+00
12.25	.383E+00	.101E+00	.373E+00	.902E-01
12.75	.461E+00	.151E+00	.625E+00	.193E+00
13.25	.477E+00	.186E+00	.330E+00	.141E+00
13.75	.217E+00	.973E-01	.104E+00	.768E-01
14.25	.120E+00	.946E-01	.169E+00	.102E+00
14.75	.204E+00	.133E+00	.655E-01	.714E-01
Mass(GeV)	$x_F = 0.325$	Error	$x_F = 0.375$	Error
4.75	.131E+02	.118E+01	.121E+02	.157E+01
5.25	.123E+02	.455E+00	.100E+02	.456E+00
5.75	.900E+01	.337E+00	.723E+01	.317E+00
6.25	.707E+01	.283E+00	.582E+01	.270E+00
6.75	.600E+01	.262E+00	.438E+01	.222E+00
7.25	.495E+01	.237E+00	.367E+01	.204E+00
7.75	.420E+01	.220E+00	.355E+01	.206E+00
8.25	.303E+01	.183E+00	.236E+01	.152E+00
8.75	.279E+01	.190E+00	.208E+01	.152E+00
11.25	.611E+00	.112E+00	.629E+00	.112E+00
11.75	.622E+00	.110E+00	.359E+00	.767E-01
12.25	.413E+00	.921E-01	.258E+00	.674E-01
12.75	.319E+00	.843E-01	.330E+00	.926E-01
13.25	.201E+00	.696E-01	.254E+00	.979E-01
13.75	.584E-01	.386E-01	.233E+00	.109E+00
14.25	.718E+00	.379E+00	.465E-01	.482E-01

Mass(GeV)	$x_F = 0.425$	Error	$x_F = 0.475$	Error
4.75	.131E+02	.238E+01	.827E+01	.261E+01
5.25	.818E+01	.485E+00	.740E+01	.627E+00
5.75	.616E+01	.342E+00	.527E+01	.383E+00
6.25	.504E+01	.285E+00	.367E+01	.244E+00
6.75	.384E+01	.222E+00	.306E+01	.225E+00
7.25	.275E+01	.176E+00	.223E+01	.165E+00
7.75	.232E+01	.159E+00	.173E+01	.138E+00
8.25	.238E+01	.179E+00	.150E+01	.139E+00
8.75	.210E+01	.170E+00	.146E+01	.145E+00
11.25	.358E+00	.677E-01	.273E+00	.576E-01
11.75	.362E+00	.950E-01	.415E+00	.103E+00
12.25	.294E+00	.743E-01	.188E+00	.569E-01
12.75	.314E+00	.950E-01	.202E+00	.728E-01
13.25	.217E+00	.102E+00	.114E+00	.690E-01
13.75	.701E-01	.414E-01	.857E-01	.469E-01
14.25	.130E+00	.883E-01	.505E-01	.535E-01
14.75	.298E+00	.255E+00	.725E-01	.624E-01
15.25	.460E-01	.369E-01	.000E+00	.000E+00
15.75	.113E+00	.875E-01	.000E+00	.000E+00
Mass(GeV)	$x_F = 0.525$	Error	$x_F = 0.575$	Error
5.25	.523E+01	.568E+00	.446E+01	.874E+00
5.75	.392E+01	.366E+00	.355E+01	.469E+00
6.25	.223E+01	.193E+00	.179E+01	.180E+00
6.75	.206E+01	.172E+00	.193E+01	.225E+00
7.25	.181E+01	.168E+00	.116E+01	.135E+00
7.75	.119E+01	.122E+00	.936E+00	.114E+00
8.25	.855E+00	.993E-01	.664E+00	.861E-01
8.75	.931E+00	.113E+00	.506E+00	.812E-01
11.25	.316E+00	.792E-01	.341E-01	.155E-01
11.75	.368E+00	.107E+00	.164E-01	.120E-01
12.25	.145E+00	.725E-01	.897E-01	.417E-01
12.75	.769E-01	.534E-01	.448E-01	.314E-01
13.25	.673E-01	.334E-01	.805E-01	.643E-01
13.75	.802E-01	.511E-01	.659E-01	.423E-01
14.25	.643E-01	.471E-01	.422E-01	.455E-01
14.75	.173E+00	.128E+00	.000E+00	.000E+00

Mass(GeV)	$x_F = 0.625$	Error	$x_F = 0.675$	Error
5.25	.200E+01	.537E+00	.126E+01	.604E+00
5.75	.266E+01	.484E+00	.479E+00	.192E+00
6.25	.108E+01	.159E+00	.917E+00	.246E+00
6.75	.855E+00	.122E+00	.449E+00	.102E+00
7.25	.740E+00	.131E+00	.718E+00	.166E+00
7.75	.586E+00	.103E+00	.185E+00	.443E-01
8.25	.345E+00	.713E-01	.267E+00	.769E-01
8.75	.342E+00	.893E-01	.952E-01	.444E-01
11.25	.575E-01	.310E-01	.535E-01	.308E-01
11.75	.657E-01	.485E-01	.000E+00	.000E+00
12.25	.225E+00	.156E+00	.253E-01	.210E-01
12.75	.301E-01	.288E-01	.384E-01	.436E-01
13.25	.716E-01	.529E-01	.000E+00	.000E+00

Table II. Invariant cross section in nb/GeV^2/nucleon for 1 GeV wide mass bins. Cross sections correspond to the range $0.1 \leq x_F \leq 0.3$. Only statistical errors are listed; total error includes an additional $\pm 10\%$ systematic error described in the text.

p_t (GeV)	Mass = 5.5 GeV	Error	Mass = 6.5 GeV	Error
.125	.157E+01	.708E-01	.666E+00	.355E-01
.375	.133E+01	.372E-01	.537E+00	.181E-01
.625	.120E+01	.301E-01	.506E+00	.152E-01
.875	.906E+00	.234E-01	.344E+00	.105E-01
1.125	.705E+00	.212E-01	.282E+00	.952E-02
1.375	.524E+00	.198E-01	.188E+00	.774E-02
1.625	.358E+00	.170E-01	.118E+00	.603E-02
1.875	.273E+00	.210E-01	.822E-01	.542E-02
2.125	.926E-01	.107E-01	.714E-01	.678E-02
2.375	.131E+00	.218E-01	.416E-01	.533E-02
2.625	.572E-01	.134E-01	.367E-01	.807E-02
2.875	.193E-01	.652E-02	.148E-01	.358E-02
3.125	.000E+00	.000E+00	.950E-02	.327E-02
3.375	.000E+00	.000E+00	.149E-01	.184E-01
3.625	-.612E-02	.203E-02	.480E-02	.401E-02
3.875	.000E+00	.000E+00	.235E-03	.203E-03
p_t (GeV)	Mass = 7.5 GeV	Error	Mass = 8.5 GeV	Error
.125	.389E+00	.278E-01	.175E+00	.175E-01
.375	.274E+00	.120E-01	.150E+00	.861E-02
.625	.234E+00	.872E-02	.109E+00	.549E-02
.875	.182E+00	.693E-02	.955E-01	.474E-02
1.125	.139E+00	.584E-02	.610E-01	.334E-02
1.375	.976E-01	.483E-02	.459E-01	.279E-02
1.625	.645E-01	.404E-02	.335E-01	.241E-02
1.875	.393E-01	.302E-02	.217E-01	.205E-02
2.125	.272E-01	.289E-02	.133E-01	.170E-02
2.375	.166E-01	.238E-02	.638E-02	.110E-02
2.625	.120E-01	.240E-02	.403E-02	.936E-03
2.875	.109E-01	.352E-02	.246E-02	.876E-03
3.125	.328E-02	.123E-02	.119E-02	.912E-03
3.375	.233E-02	.153E-02	.255E-02	.229E-02

p_t (GeV)	Mass = 11.5 GeV	Error	Mass = 12.5 GeV	Error
.125	.201E-01	.683E-02	.677E-02	.499E-02
.375	.214E-01	.395E-02	.429E-02	.159E-02
.625	.893E-02	.182E-02	.687E-02	.183E-02
.875	.899E-02	.155E-02	.653E-02	.144E-02
1.125	.885E-02	.133E-02	.511E-02	.112E-02
1.375	.392E-02	.866E-03	.182E-02	.521E-03
1.625	.288E-02	.651E-03	.180E-02	.655E-03
1.875	.255E-02	.662E-03	.495E-03	.233E-03
2.125	.141E-02	.439E-03	.569E-03	.402E-03
2.375	.496E-03	.237E-03	.510E-03	.359E-03
2.625	.434E-03	.263E-03	.755E-03	.597E-03
p_t (GeV)	Mass = 13.5 GeV	Error	Mass = 14.5 GeV	Error
.125	.528E-02	.413E-02	.355E-02	.481E-02
.375	.156E-02	.857E-03	.185E-02	.118E-02
.625	.106E-02	.553E-03	.000E+00	.000E+00
.875	.236E-02	.104E-02	.180E-02	.922E-03
1.125	.159E-02	.814E-03	.704E-03	.416E-03
1.375	.134E-02	.565E-03	.172E-02	.175E-02
1.625	.236E-03	.158E-03	.685E-03	.461E-03

Table III. Production cross section times the branching ratio for decay into dimuons for the $\Upsilon(1S)$ state versus x_F in pb/nucleon for $p_t \leq 4$ GeV. Only statistical errors are listed; total error includes an additional $\pm 10\%$ systematic error described in the text.

x_F	$B \times d\sigma/dx_F$	Error
-0.05	7.351E+00	5.748E-01
0.05	5.956E+00	2.671E-01
0.15	4.750E+00	1.765E-01
0.25	3.550E+00	1.394E-01
0.35	2.159E+00	1.045E-01
0.5	3.013E-01	2.643E-02

Table IV. Production cross section times the branching ratio for decay into dimuons for the $\Upsilon(1S)$ state versus p_t in pb/GeV^2/nucleon. The data have been integrated over the range, $-0.1 \leq x_F \leq 0.6$. Only statistical errors are listed; total error includes an additional $\pm 10\%$ systematic error described in the text.

p_t (GeV)	$\frac{B \times E}{\pi\sqrt{s}} \times \frac{1}{p_t} d\sigma/dp_t$	Error
0.25	2.155E-01	1.616E-02
0.50	2.370E-01	1.050E-02
0.75	1.765E-01	8.529E-03
1.25	8.338E-02	4.620E-03
1.50	7.360E-02	3.310E-03
1.75	3.450E-02	3.190E-03
2.00	1.715E-02	1.380E-03
2.25	1.260E-02	1.600E-03
2.50	1.580E-02	1.470E-03
3.00	3.530E-03	5.333E-04
3.50	1.300E-03	7.430E-04

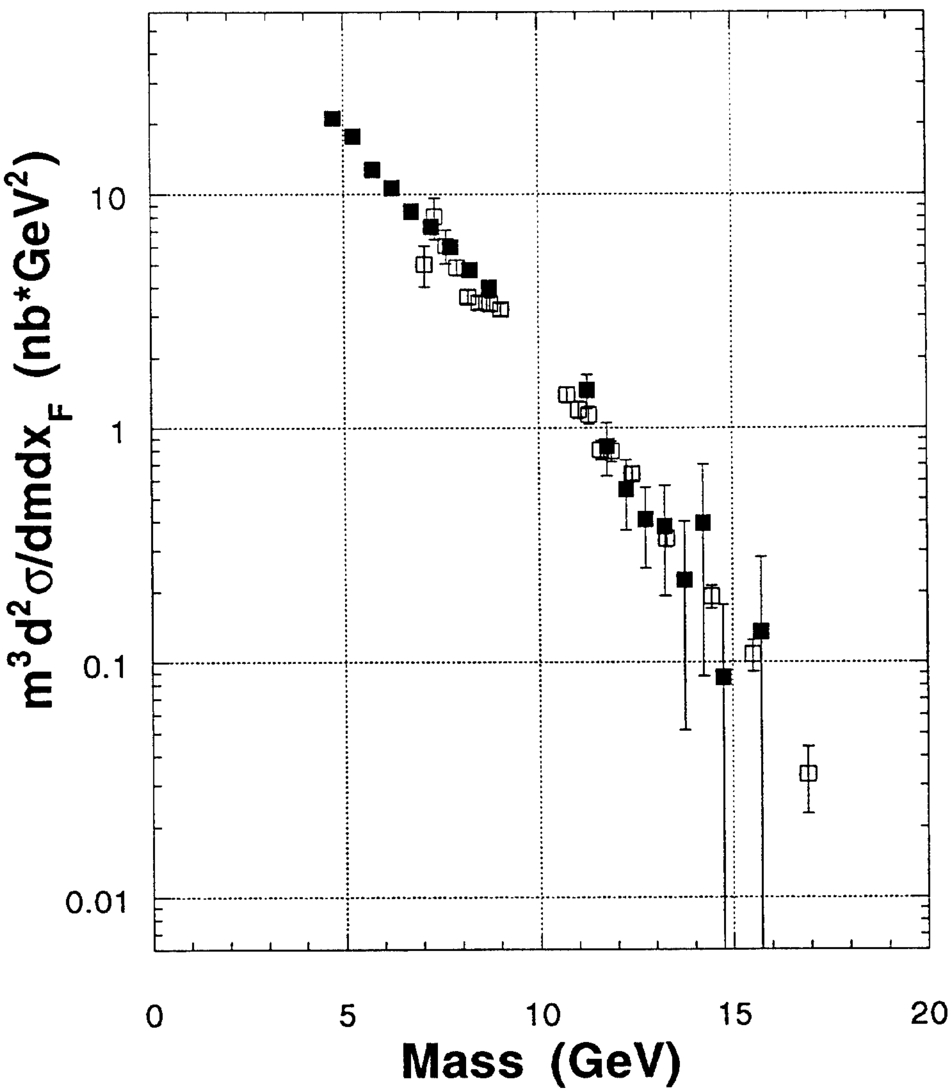

$m^3 d^2\sigma/dmdx_F$ (nb*GeV^2)
10
1
0.1
0.01
0
5
10
15
20
Mass (GeV)

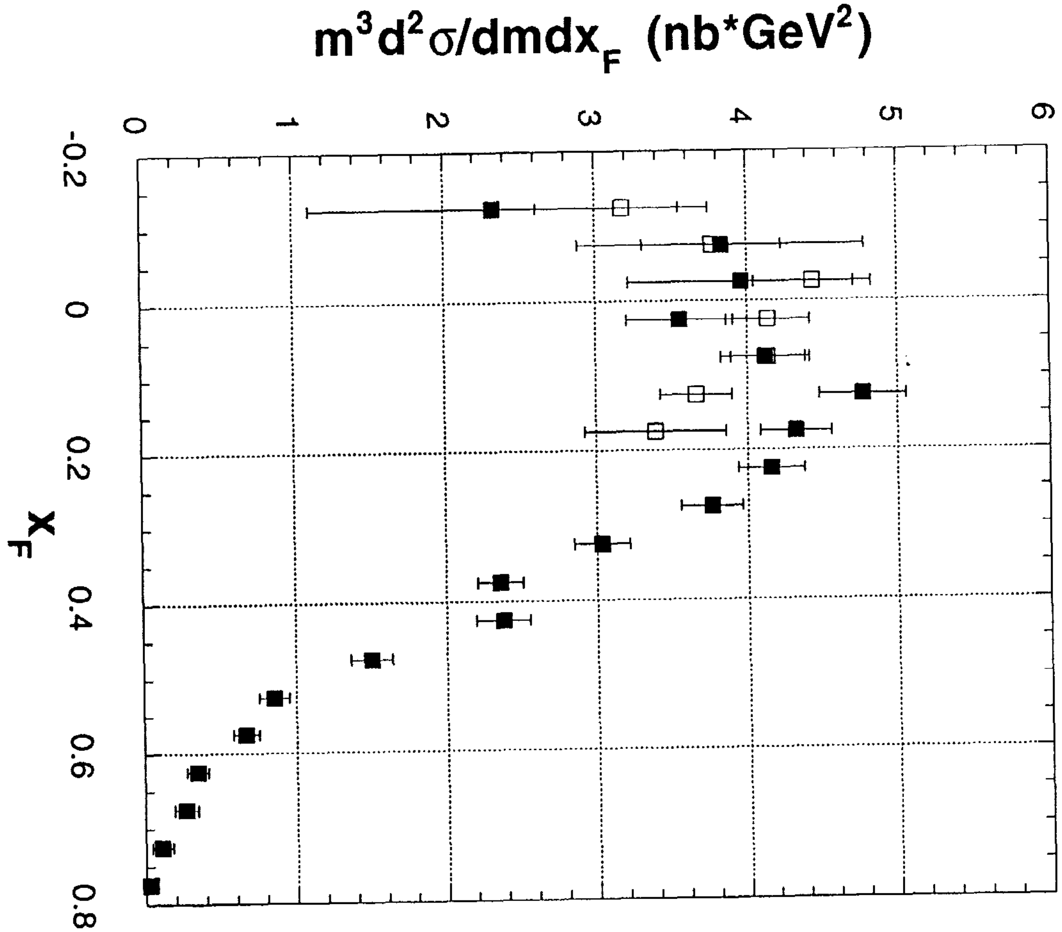

m^3d^2σ/dmdx_F (nb*GeV^2)
x_F
0
1
2
3
4
5
6
-0.2
0
0.2
0.4
0.6
0.8

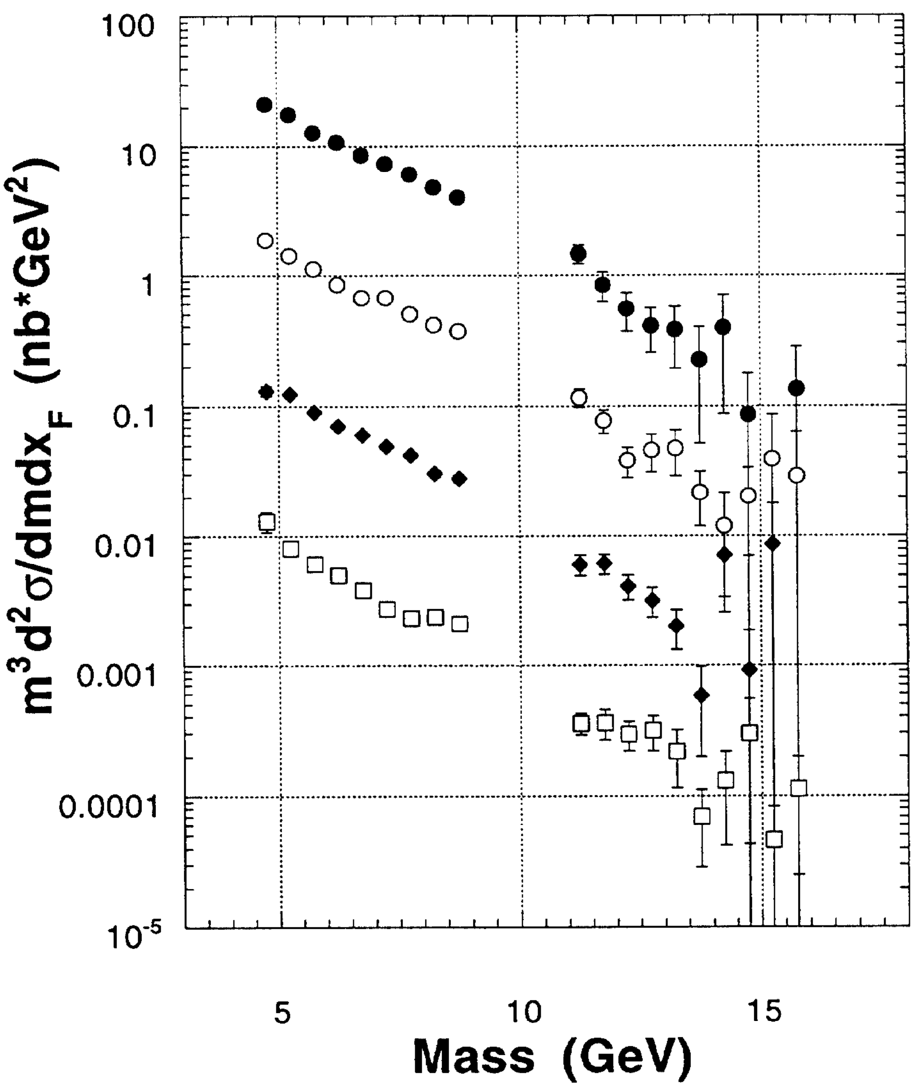
100
10
1
0.1
0.01
0.001
0.0001
10^-5
m^3d^2σ/dmdx_F (nb*GeV^2)
5
10
15
Mass (GeV)

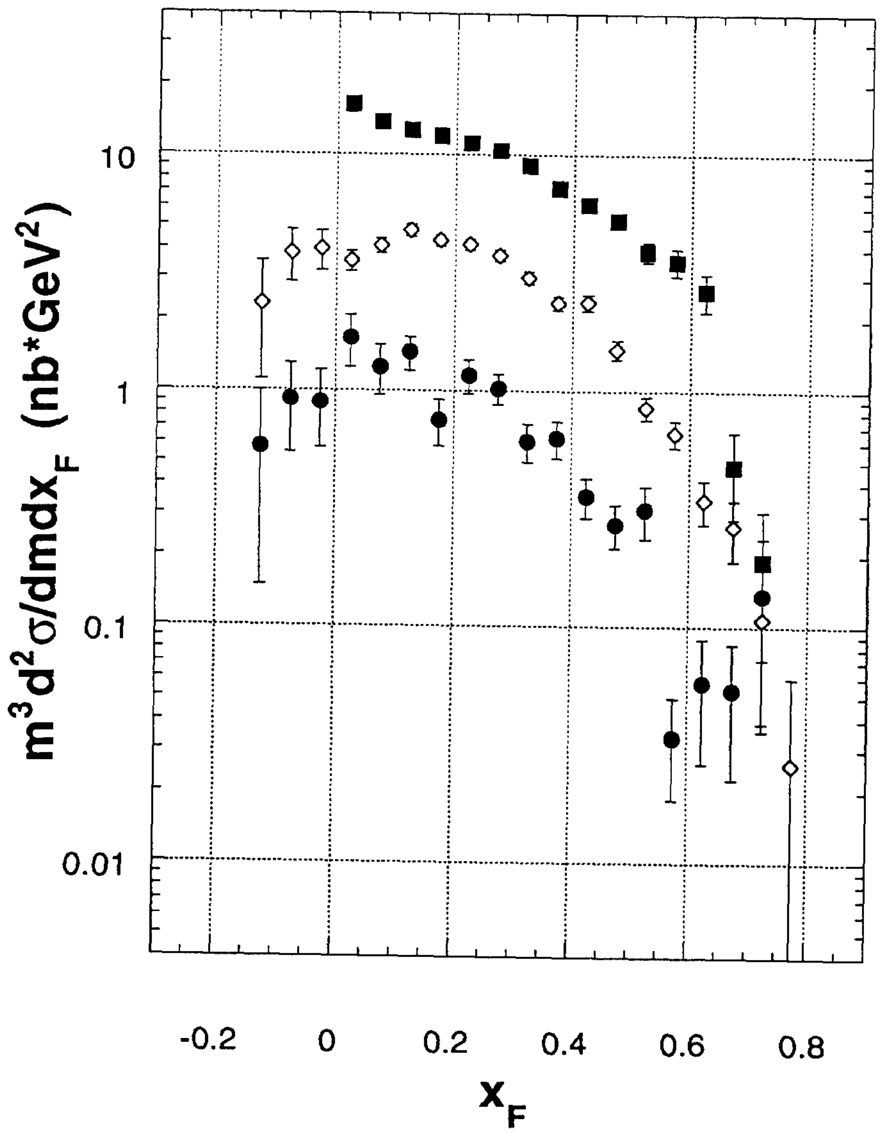

10
1
0.1
0.01
$m^3 d^2\sigma/dmdx_F$ (nb*GeV^2)
-0.2
0
0.2
0.4
0.6
0.8
x_F

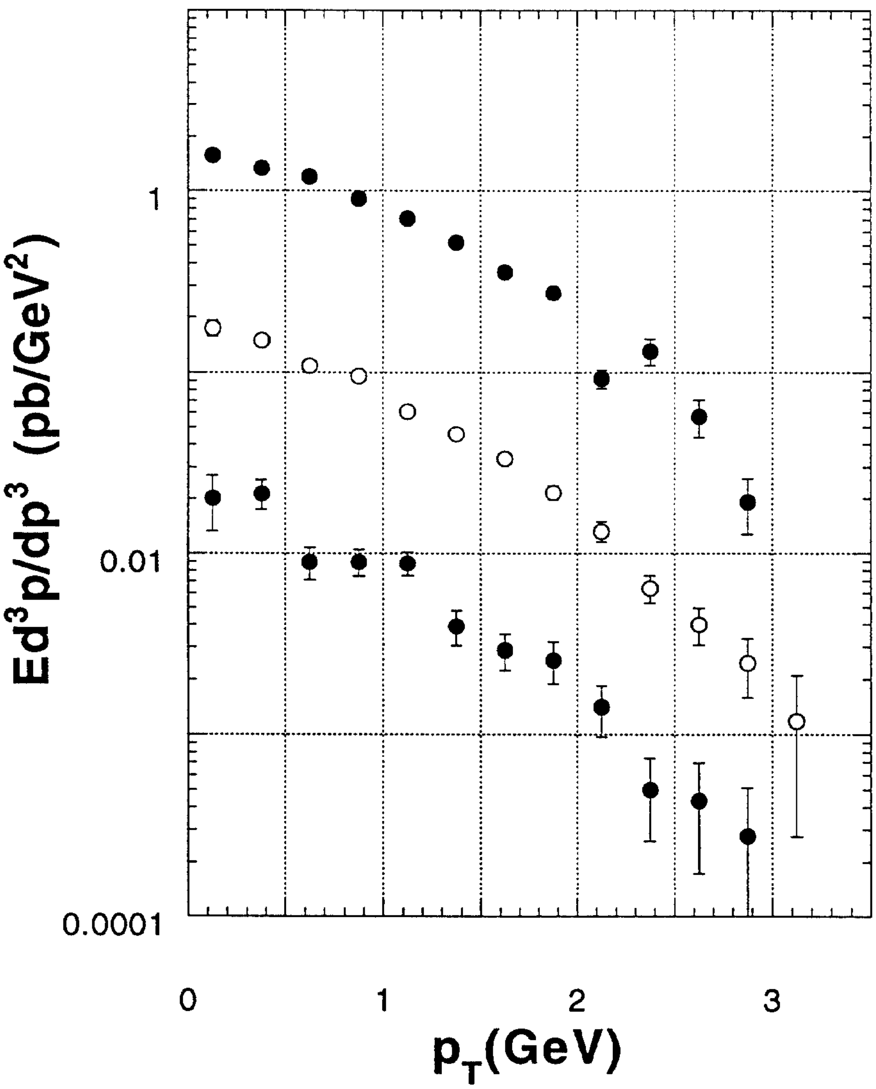

1
0.01
0.0001
0
1
2
3
Ed^3p/dp^3 (pb/GeV^2)
p_T(GeV)